Incidental Adrenal Lesions: Principles, Techniques, and Algorithms for Imaging Characterization[1]

Giles W. L. Boland, MD
Michael A. Blake, MD
Peter F. Hahn, MD, PhD
William W. Mayo-Smith, MD

Incidental adrenal lesions are commonly detected at computed tomography, and lesion characterization is critical, particularly in the oncologic patient. Imaging tests have been developed that can accurately differentiate these lesions by using a variety of principles and techniques, and each is discussed in turn. An imaging algorithm is provided to guide radiologists toward the appropriate test to make the correct diagnosis.

[1] From the Department of Radiology, Massachusetts General Hospital, White Building 270C, 55 Fruit St, Boston, MA 02114 (G.W.L.B., M.A.B., P.F.H.); and Department of Radiology, Warren Alpert Medical School of Brown University, Rhode Island Hospital, Providence, RI (W.W.M.). Received June 5, 2007; revision requested August 6; revision received August 31; accepted January 16, 2008; final version accepted February 27. **Address correspondence to** G.W.L.B. (e-mail: *gboland@partners.org*).

Radiology

The incidental adrenal lesion (IAL), or incidentaloma, is an adrenal mass, usually 1 cm or larger in size (1). Typically these lesions are discovered during computed tomography (CT) performed for indications other than adrenal disease but are occasionally detected at magnetic resonance (MR) imaging, positron emission tomography (PET), or even ultrasonography (US). With the increasing use of imaging, IALs are being more frequently detected and are seen in approximately 4%–6% of the imaged population (2–4). Almost all of these lesions will prove to be benign in a patient without a known history of cancer (4–9). On the other hand, once the patient has a diagnosis of an extraadrenal malignancy, the chance that an incidentally detected adrenal mass is malignant increases substantially (1). Characterization of the IAL in these patients is essential to predict the prognosis of the primary disease, to assess staging, and to direct therapy. The radiologist plays a critical role in the characterization of these adrenal lesions.

Essentials

- Almost all incidental adrenal lesions (IALs) in patients without a known primary cancer are benign.
- Characterization of IALs in patients with cancer is essential to predict prognosis of the primary disease, to assess staging, and to direct therapy.
- Almost all IALs can be characterized by using imaging alone, although some lesions will require percutaneous biopsy for definitive characterization.
- Characterization depends on lesion morphology, perfusion differences between benign and malignant masses, the intracellular lipid concentration of the mass, and the metabolic activity of the mass.
- CT contrast medium washout tests offer the highest test sensitivity and specificity for IAL characterization.

This review will discuss the anatomic and physiologic imaging principles used for differentiating adrenal masses, present the imaging techniques available to the radiologist, and recommend an imaging algorithm that can guide the radiologist toward the correct diagnosis.

Prevalence and Causes of IAL

Adrenal lesions can be categorized as primary or metastatic, benign or malignant, and functioning or nonfunctioning (1). Their precise frequency and distribution is unclear, as results in reported series vary in the observed rate of different adrenal pathologic conditions. Adenomatous lesions are detected on approximately 0.2% of CT scans in patients aged 20–29 years, as compared with 7%–10% in elderly patients (1,3,6,7). Of these lesions, approximately 94% will be nonfunctioning cortical adenomas, and 6% will be functioning due to autonomous cortisol-secreting (5%) and aldosterone- or sex hormone–producing tumors (1%) (1–3). Other benign lesions include myelolipoma (9% of detected lesions) and adrenal cysts, hemorrhage, ganglioneuroma, hemangioma, neuroblastoma, and granulomatous disease, which compose perhaps 1%–2% combined of all IALs (Table 1) (1–4).

According to the literature, IALs that are determined to be malignant account for approximately 2%–3% of all detected lesions, which will also increase in number and proportion with patient age (1). However, other reports state this number to be much higher (up to 30%), but this likely reflects clinical practices that are more oncology based (3). Some reports indicate that adrenal carcinoma (5%) and pheochromocytoma (5%) are more commonly seen than metastatic disease, while others state that metastatic disease is far more common (1,3,7). In most clinical practices, however, adrenal carcinomas and pheochromocytomas are uncommon tumors, probably accounting for fewer than 5% combined of all detected IALs (10). Other rare adrenal malignancies include primary lymphoma of the adrenal glands, hemangiosarcoma, and neuroblastoma (11).

Authors agree, however, that the chance of an IAL proving to be malignant is highly dependent on whether the patient has an underlying extraadrenal malignancy. Up to 27% of oncologic patients will have microscopic adrenal metastases, and approximately 50% of incidentally detected adrenal lesions in cancer patients will represent metastatic disease (1,3,8,12).

Principles of Adrenal Imaging

Once an IAL has been detected, its characterization will depend on whether it is benign or malignant and functioning or nonfunctioning. Functioning cortical adenomas and pheochromocytomas are best characterized by means of biochemical assays.

The most common clinical conundrum is to differentiate benign nonfunctioning adenomas from malignant disease. The strength and practicality of any imaging test devised to differentiate these lesions will ultimately depend on its test sensitivity and specificity. First, the test needs to be sufficiently sensitive to detect focal adrenal lesions when present. However, while high sensitivity is useful, the critical characteristic of an imaging test is its ability to characterize adrenal lesions—that is, to distinguish those that require further evaluation from those that can be safely left alone. For instance, characterization of an IAL as an adenoma in a patient with lung cancer and no other CT evidence of metastatic disease would indicate curative therapy for the primary lung disease. An adrenal metastasis, on the

Published online
10.1148/radiol.2493070976

Radiology 2008; 249:756–775

Abbreviations:
APW = absolute percentage washout
FDG = fluorodeoxyglucose
IAL = incidental adrenal lesion
MIBG = *m*-iodobenzylguanidine
ROI = region of interest
RPW = relative percentage washout

Authors stated no financial relationship to disclose.

Table 1

Morphologic and Imaging Characteristics of IALs

IAL	Frequency (%)	Size (cm)	Shape	Texture	Growth Rate	Unenhanced CT Attenuation (HU)	15-minute CT Washout (%)	MR SI Characteristics	Nuclear Medicine Characteristics
Adenoma	About 50–80 (common)	1–4	Smooth, round	Homogeneous	Stable or very slow	<10 in 70%	RPW > 40; APW > 60	SI drop off on opposed-phase images	Negative on PET images
Metastasis	Uncommon unless patient has cancer	Variable, usually <3	Variable	Heterogeneous when larger	Variable, slow to rapid	>10	RPW < 40	May show increased SI on T2-weighted images	Positive on PET images
Myelolipoma	5–10	1–5	Smooth, round	Variable, with macroscopic fat	Stable to slow	<0, often <−50	No data available	Variable SI drop off on opposed-phase images	Negative on PET images
Lymphoma	Rare as primary, more common as metastasis	Variable	Variable	Variable	Variable, slow to rapid	>10	RPW < 40	Intermediate SI	Variable positivity on PET images
Carcinoma	<5 (rare)	Usually >4	Variable	Variable	Variable, usually slow	>10	RPW < 40	Intermediate SI	Positive on PET images
Pheochromocytoma	5	Variable	Variable	Variable	Slow	>10, rarely <10	RPW < 40	High SI on T2-weighted images	Positive on MIBG images
Hematoma	1	Variable	Smooth	Variable	Rapid	>10, sometimes >50	No data available	Variable SI	Negative
Cyst	1	Variable	Smooth, round	Homogeneous	Usually stable	<10	Does not enhance	High SI on T2-weighted images	Negative
Neuroblastoma	Rare, more common in children	Variable, but often large	Variable	Variable	Variable, slow to rapid	>10	RPW < 40	Variable if necrotic	Positive
Ganglioneuroma	Very rare	Variable	Variable	Variable	Variable, slow to rapid	>10	No data available	Usually intermediate SI	Usually negative
Hemangioma	Very rare	Variable	Variable	Variable	Usually slow	>10	No data available	Usually intermediate SI	Usually negative
Granulomatous	Rare outside Asia	1–5	Smooth	Usually homogeneous	Variable, slow to intermediate	>10	No data available	Usually intermediate SI	Positive on PET images if active

Note.—APW = absolute percentage washout, MIBG = m-iodobenzylguanidine, RPW = relative percentage washout, SI = signal intensity.

other hand, would usually direct treatment toward palliative care. Hence, incorrect lesion characterization could have unfortunate consequences for the patient.

High test specificity is, therefore, the crux of adrenal imaging, and tests must be devised that are as close to 100% specific as possible (13). Ideally, for the test to be useful in clinical practice, it should also be reasonably sensitive; however, it is far safer to leave some lesions uncharacterized rather than risk making a diagnosis of benignity in error.

A number of imaging tests have now been developed that attempt to address these strict test criteria. Morphologic imaging, while sometimes helpful, is often limited by its poor test specificity. Fortunately, other imaging techniques have been more recently devised that do meet the test criteria. These tests, which make use of CT, MR imaging, and PET, exploit three fundamentally different physiologic principles: *(a)* the intracellular lipid concentration of the mass, *(b)* the perfusion differences between benign and malignant masses, and *(c)* the metabolic activity of the mass. The importance of adrenal imaging methods continues to evolve, and each method will be discussed in turn.

Morphologic Imaging: CT and MR Imaging

The structural features of most IALs are not specific enough for them to be characterized with anatomic imaging tests (CT or MR) alone, particularly as most lesions will be small (1–3 cm) when discovered and smooth and uniform in shape, regardless of their histologic characteristics (Fig 1). Lesion characterization will usually depend on other imaging principles, although some imaging morphologic features can be helpful, if used with caution.

Perhaps the most useful principle that can aid characterization of IALs is evaluation of any relevant prior imaging test results. As a rule of thumb, any adrenal lesion that increases in size on serial images (usually obtained 6 months apart) can be considered malignant. Caveats to this statement include some benign lesions (adenomas and myelolipomas) that can increase in size very slightly over this time period in rare cases. Furthermore, hemorrhage into the adrenal gland, whether traumatic or spontaneous (as in myelolipomas) will cause abrupt adrenal enlargement (14,15). In practice, however, any increase in size is generally considered malignant until proved otherwise. Conversely, stability of a lesion signifies benignity. It is highly unusual for untreated malignant lesions to demonstrate stability on 6-month follow-up images (4,8).

Furthermore, larger lesions are much more likely to be malignant (1). Once an IAL is larger 4 cm, the chance that it is malignant increases to approximately 70% (85% if larger than 6 cm) (1,3). Some authors have placed these percentages much lower, but it is unusual in clinical practice to see benign lesions larger than 4 cm (4). For lesions larger than 4–5 cm, adrenal adenocarcinoma should be strongly considered, particularly if the patient has no other history of malignancy (16). Some myelolipomas are also large but are confidently recognized owing to the presence of macroscopic fat (1,4, 14,15).

Both benign and malignant lesions can be heterogeneous in attenuation, particularly after the administration of intravenous contrast medium (Fig 2). Large necrotic areas in a lesion usually signify malignancy. Conversely, metastases, when detected, are often homogeneous and similar in appearance to adenomas, especially when small (Fig 1). Most adrenal cysts, owing to their uniform and homogeneous nature, can be characterized morphologically, although some can be complex

Figure 1

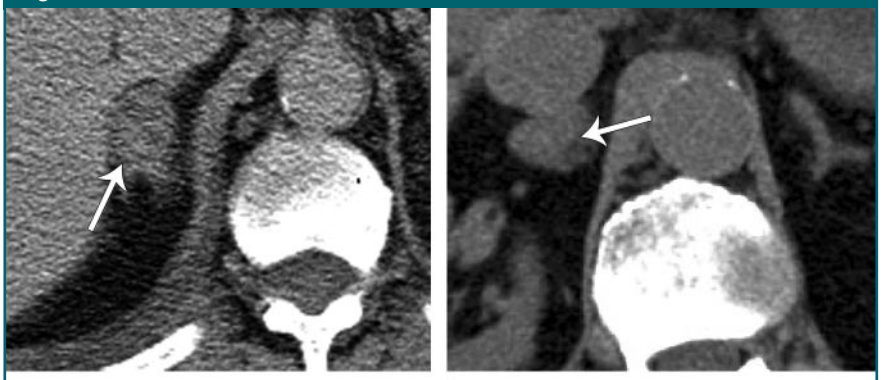

a. b.

Figure 1: Common appearance of many IALs when detected. **(a)** Axial contrast medium–enhanced CT scan shows 1.8-cm uniform right adrenal adenoma (arrow) in 44-year-old man with colorectal cancer. Morphologic features cannot be used to differentiate this from metastasis. **(b)** Axial unenhanced CT scan shows 1.5-cm uniform right adrenal metastasis (arrow) in 75-year-old man with lung cancer. Appearance is similar to that of many adenomas.

Figure 2

Figure 2: Axial contrast-enhanced CT scan demonstrates 5.8-cm irregular heterogeneous right adrenal metastasis (arrow) that invades adjacent liver in 51-year-old woman with lung cancer.

Figure 3

Figure 3: Axial unenhanced CT scan shows 1.6-cm proved left adrenal adenoma with exophytic component (arrow) in 71-year-old man with colorectal cancer.

Figure 4

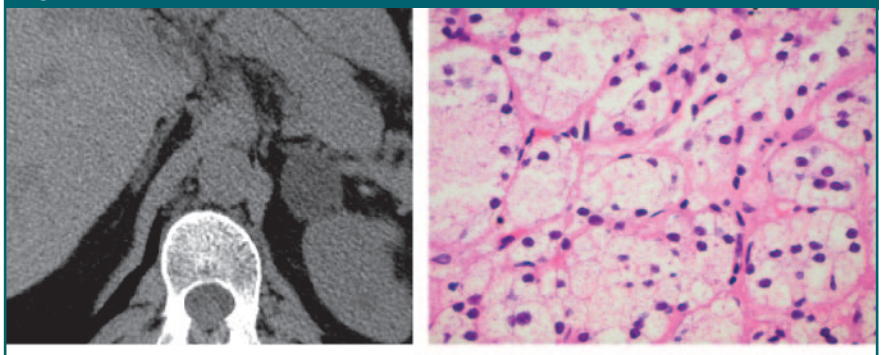

a. b.

Figure 4: Biopsy-proved lipid-rich left adrenal adenoma in 51-year-old man with lung cancer. **(a)** Axial unenhanced CT scan shows 2.4-cm mass with attenuation of 3 HU. **(b)** High-power photomicrograph of left adrenal histologic specimen. Adenoma cells have small nuclei and finely vacuolated (lipid rich) cytoplasm. (Hematoxylin-eosin stain; original magnification, ×60.) (Image courtesy of Martha Pitman, MD.)

and are occasionally confused with necrotic adrenal carcinomas (4,8,17).

The shape or margination of the adrenal lesion can sometimes be helpful, because large lesions with highly irregular borders are usually malignant (Fig 2). Some adenomas, however, also demonstrate irregularity, and, even in patients with an extraadrenal malignancy adrenal multinodularity is usually associated with benignity (Fig 3) (18).

Lipid-sensitive Imaging Techniques: CT and MR Imaging

Lipid-sensitive imaging tests exploit the fact that up to 70% of adrenal adenomas contain abundant intracellular fat (mainly cholesterol, fatty acids, and neutral fat), whereas almost all malignant lesions do not (19–24). Both CT and MR lipid-sensitive imaging techniques have been proved to be highly effective at characterizing this subset of lesions.

CT Techniques

Lee et al (22) in 1991 reported conclusively that unenhanced CT densitometry could effectively differentiate many adrenal adenomas from nonadenomatous disease. In that study, the authors found that the mean attenuation of adrenal adenomas (−2.2 HU) was significantly lower than that of nonadenomas (28.9 HU). By using an attenuation threshold of 0 HU, these lesions could be then differentiated with a sensitivity and specificity of 47% and 100%, respectively. Later, Korobkin et al (19) demonstrated that this phenomenon is related to the intracellular fat concentration in adrenal adenomas and that there is an inverse linear relationship between fat concentration and attenuation on unenhanced CT images (Fig 4). Conversely, almost all nonadenomatous lesions are deficient of intracellular fat, and their CT attenuation values are consequently higher.

The CT densitometry technique involves placement of a region of interest (ROI) over the adrenal gland, avoiding necrotic or hemorrhagic areas (4, 19,23). The measurement should be made on a CT section through the center of the lesion, to avoid partial-volume effects from adjacent retroperitoneal fat (Fig 5). Typically the ROI should be placed over one-half to two-thirds of the lesion surface area, to decrease noise artifact and avoid spurious pixel numbers that can be seen with small ROIs (4,19,23,24).

A pooled analysis (13) of multiple published studies later corroborated the initial findings of Lee et al (22) and found that if the CT attenuation threshold is raised to 10 HU, the test sensitivity becomes far higher (71%) while high specificity (98%) is maintained. Therefore only two of 100 adrenal lesions with an attenuation value of less than 10 HU on unenhanced CT scans will be nonadenomatous. Fortunately, these lesions can often be characterized by other means. The 10-HU threshold is now used as a standard reference point from which lipid-rich adenomas can be differentiated from other adrenal lesions on unenhanced CT scans.

Figure 5

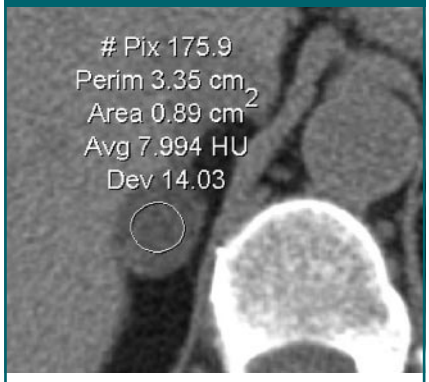

Figure 5: Axial unenhanced CT scan shows 1.8-cm right adrenal mass in 63-year-old woman. Circular ROI over one-half of lesion surface area yields attenuation measurement *(Avg)* of about 8 HU, virtually excluding metastatic disease. Other data in ROI include standard deviation *(Dev)* of attenuation, number of pixels *(#Pix)*, circumference *(Perim)*, and area.

Limitations to this test persist, however. First, up to 30% of adenomas are lipid poor and have an attenuation value greater than 10 HU on unenhanced CT scans, as do almost all malignant lesions

(4,8,22,23,26–30). Therefore, all lesions above 10 HU on an unenhanced CT scan are considered indeterminate, and other tests are generally required to characterize them. Second, most abdominal and chest CT scans are now obtained with the use of intravenous contrast medium; thus, unenhanced attenuation measurements cannot be made. Many studies (23,25–30) have demonstrated that adenomas and nonadenomas enhance unpredictably and that there is too much overlap of their attenuation values for a useful dynamic contrast-enhanced CT attenuation threshold to be found.

More recently, some authors have suggested that lesions can be characterized more accurately by using a CT histogram analysis method. Bae et al (31) described this histogram method to be far more sensitive than the 10-HU threshold method for the diagnosis of adrenal adenoma on both unenhanced and enhanced CT scans. The technique relies on the supposition that most adenomas (whether lipid rich or lipid poor) contain sufficient intracytoplasmic fat to be detected and consequently characterized.

The technique again involves placement of an ROI over approximately one-half to two-thirds of the adrenal surface area. This ROI is then processed with a histogram analysis tool, which is standard on most CT viewing workstations (31). This permits measurement of the number and range of pixel attenuation measurements, which can then be visualized graphically with pixel attenuation along the x axis and pixel frequency along the y axis (Fig 6). As some nonadenomatous lesions can occasionally contain negative-attenuation pixels (<0 HU), Bae et al (31) proposed that, to maintain high test specificity, lesions should only be considered benign if the negative pixel count is greater than 10%. Other authors (32,33), however, have found the test sensitivity to be too low (71% and 12% for unenhanced and contrast-enhanced CT, respectively) to be used in routine clinical practice. Indeed, most departments do not routinely use the histogram analysis method, and its future use remains uncertain (33).

Figure 6

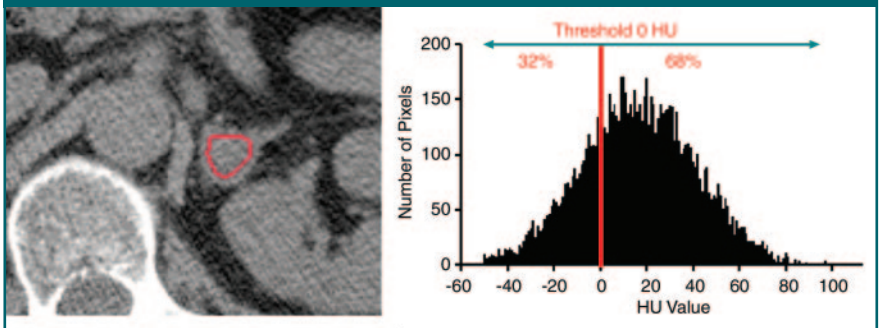

Figure 6: Lipid-poor left adrenal adenoma (20 HU) in 46-year-old woman. **(a)** Axial unenhanced CT scan with ROI (red) placed over mass for histogram analysis. **(b)** Histogram of lesion with pixel attenuation plotted against pixel number. Negative pixel count is 32%, consistent with adenoma. (Images courtesy of Nagaraj Holakere, MD.)

MR Imaging Techniques

Chemical shift MR imaging, similar to CT densitometry, is also dependent on the detection of intracellular lipid in adenomas, but chemical shift MR does so by relying on the different resonant frequencies of fat and water protons in a given voxel rather than on attenuation differences (4,8,34–37). Fat protons precess at a lower frequency than do water protons, with the net effect being that the MR signals of water and lipid protons can cancel each other out

Figure 7

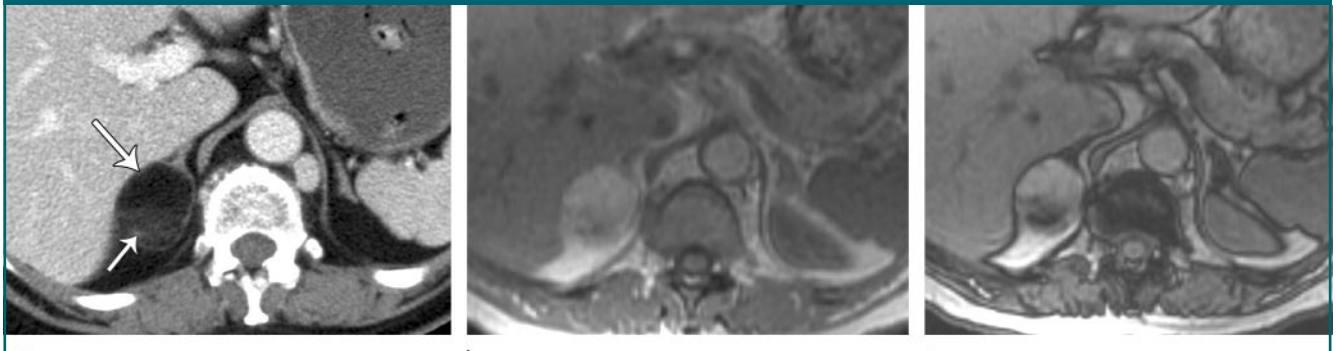

Figure 7: Myelolipoma in 46-year-old woman. **(a)** Axial contrast-enhanced CT scan shows 3.5-cm right adrenal mass composed primarily of fat anteriorly (long arrow) and mixed elements posteriorly (short arrow). **(b)** Axial T1-weighted gradient-echo in-phase MR image (repetition time msec/echo time msec, 180/4.2; 80° flip angle) shows high signal intensity anteriorly and intermediate signal intensity posteriorly. **(c)** Axial T1-weighted gradient-echo opposed-phase MR image (80/2.1, 80° flip angle) shows persistent high signal intensity anteriorly (consistent with pure fat voxels) and loss of signal intensity posteriorly (mixed fat and soft-tissue elements).

within a voxel during opposed-phase breath-hold gradient-echo MR imaging (34–38). This leads to signal intensity decrease when compared with in-phase images. Similar to the findings with unenhanced CT densitometry, Korobkin et al (19) also demonstrated there was an inverse linear relationship between the percentage of lipid-rich cells and the relative change in MR signal intensity on chemical shift images. However, the amount of signal intensity decrease will also depend on fat-to-water proton ratio within this voxel, since pure fat voxels (as often seen in myelolipomas) will show little or no signal intensity decrease on opposed-phase images because there are few, if any, water protons to cancel out the fat signal (Fig 7) (8,39). On the other hand, with almost equal voxel concentrations of fat and water protons (as seen with many lipid-rich adenomas), there will be almost complete signal intensity loss on opposed-phase chemical shift MR images (Fig 8). Lipid-poor adrenal lesions, which contain a low lipid-to-water proton ratio, cannot generally be characterized by chemical shift methods, as their signal intensity is unchanged on opposed-phase images (Fig 9). These lesions are then considered indeterminate on the basis of chemical shift MR images.

The chemical shift phenomenon can be measured quantitatively by calculating the adrenal-to-spleen chemical shift ratio. This represents the lesion-to-spleen signal intensity ratio on in-phase images divided by the lesion-to-spleen signal intensity ratio on opposed-phase images (38). A chemical shift ratio of less than 0.71 indicates a lipid-rich adenoma. Alternatively the adrenal signal intensity index can be calculated, and a measurement of more than 16.5% is also consistent with a lipid-rich adenoma (40). This index (percentage) is calculated as $[(SI_{IP} - SI_{OP})/SI_{IP}] \times 100$, where SI_{IP} and SI_{OP} are the signal intensities measured on in-phase and opposed-phase images, respectively (40). However, these quantitative techniques are cumbersome to calculate and not often used in clinical practice (41,42). Most radiologists evaluate any chemical shift change visually or qualitatively, and this has been reported to be as effective as quantitative methods (41).

When performing qualitative evaluation, the liver should not be used as the reference organ with which to determine any adrenal signal intensity decrease, because the liver will also show decreased signal intensity on opposed-phase images when there is hepatic steatosis (41). Rather, muscle or spleen should be used as the internal reference organ (8,41).

The sensitivity and specificity of chemical shift MR imaging for the differentiation of IALs are similar to those of unenhanced CT densitometry, at 81%–100% and 94%–100%, respectively, although the most rigorous qualitative study yielded a sensitivity and specificity profile of 78% and 87%, respectively (36).

Considering that the usefulness of both chemical shift MR and unenhanced CT densitometry tests are both based on the detection of intracellular lipid,

Figure 8

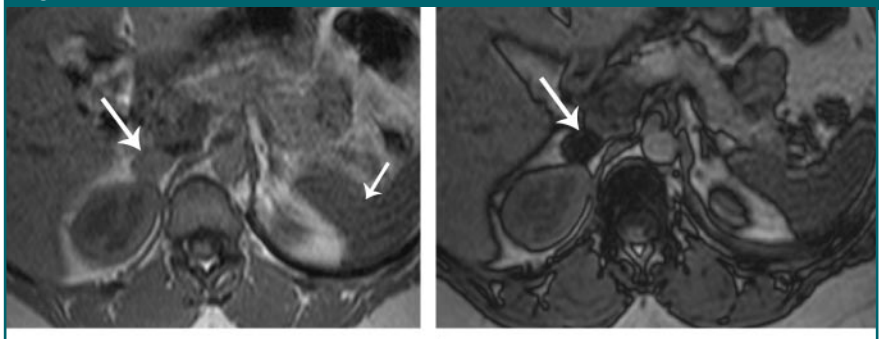

a. b.

Figure 8: Axial MR images of 2-cm right adrenal adenoma in 48-year-old man. **(a)** T1-weighted gradient-echo in-phase image (180/4.2, 80° flip angle) shows adrenal signal intensity (long arrow) slightly higher than that of spleen (short arrow) (internal reference organ). **(b)** T1-weighted gradient-echo opposed-phase image (180/2.1, 80° flip angle) shows marked signal intensity loss. Adrenal signal intensity (arrow) is markedly lower than that of spleen. (Images courtesy of Mukesh Harisinghami, MD.)

Figure 9

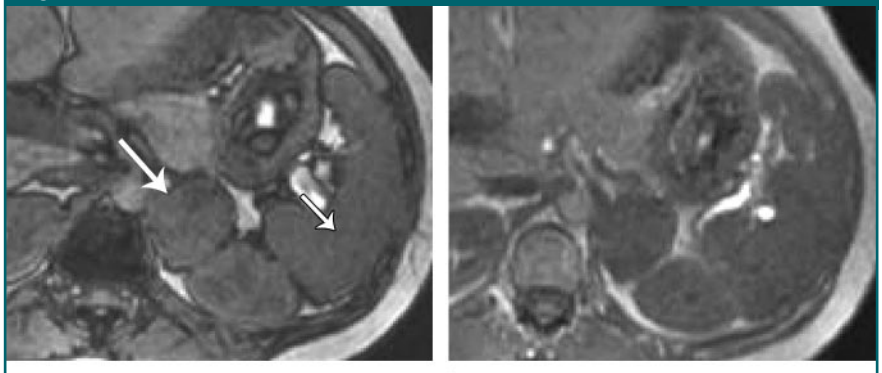

a. b.

Figure 9: Axial MR images of 4-cm left adrenal metastasis in 75-year-old woman with lung cancer. **(a)** T1-weighted gradient-echo in-phase image (180/4.2, 80° flip angle) shows signal intensity (long arrow) similar to that of spleen (short arrow). **(b)** T1-weighted gradient-echo opposed-phase image (180/2.1, 80° flip angle) shows unchanged signal intensity. Lesion is therefore indeterminate. (Images courtesy of Mukesh Harisinghami, MD.)

there has been debate as to which test might offer superior sensitivity and specificity for characterization of IALs—in particular, whether lipid-poor adenomas that cannot be characterized on unenhanced CT scans can yet be characterized on chemical shift MR images. Studies have shown that for lipid-rich adenomas, there is effectively no difference between the tests, but chemical shift imaging might be superior when evaluating lipid-poor adenomas (43). However, one study (44) demonstrated that chemical shift imaging might be useful only when the unenhanced CT attenuation is less than 30 HU.

In practice, most investigators still consider CT to be the initial test of choice, because it is more available and cheaper (4,5,45). Furthermore, CT contrast medium washout tests (discussed in next section) have proved to be the most effective diagnostic imaging tool with which to differentiate IALs (4,5,23,25,27,29,45–47).

Perfusion Imaging of the Adrenal Glands: CT Washout Scans

Several authors (24,27,28,30) observed that while the CT densitometry method was unable to characterize IALs during the dynamic phase of a contrast-enhanced examination, it could be used after a variable delay (15 minutes to 1 hour). It was noticed that intravenous contrast medium tended to "wash out" much faster, sometimes as early as 3 minutes, from adenomatous lesions than from nonadenomatous lesions and that the CT attenuation values began to approximate their unenhanced values (5).

However, as delayed CT densitometry measurements may depend on the type, total dose, and injection rate of intravenous contrast material, as well as the cardiac output of the patient, an absolute attenuation measurement on a delayed scan was not found to be very useful (4,5,23,29). Fortuitously, it was observed that the ratio of adrenal attenuation measurements on the washout-delayed scan when compared with the initial dynamic enhanced study could help characterize adrenal lesions with great precision (5,28). While this phenomenon was first noticed for MR imaging techniques, it was considered too impractical and variable to be used in clinical practice (48). Korobkin and colleagues then described a threshold enhancement washout value with the corresponding sensitivities and specificities for the diagnosis of adrenal adenoma. The percentage enhancement washout represents the percentage of the initial wash in of enhancement that is washed out at the time of delayed scanning (4,5,27). If an unenhanced scan has been obtained, an APW can be calculated. If no unenhanced scan is available, it has proved just as useful in clinical practice to calculate the RPW. Fortunately, these percentage washouts are easy to calculate by using certain equations (Table 2).

Several reports have now confirmed the accuracy of using either APW or RPW, and their use is now embedded in standard clinical practice (23,25,29,45, 47) (Table 2). Although there is some debate as to the exact percentage wash-

Table 2

Percentage Washout Formulas for 15-minute Delayed Contrast-enhanced CT Scans

Percentage Washout	Formula	Washout Values (%)	
		Adenoma	Malignancy
APW	$(E - D)/(E - U) \times 100$	>60	<60
RPW	$(E - D)/E \times 100$	>40	<40

Note.—Included are threshold percentage washout values that can be used to accurately differentiate adenoma from malignancy. D = delayed enhanced value, E = enhanced attenuation value, U = unenhanced attenuation value.

Figure 10

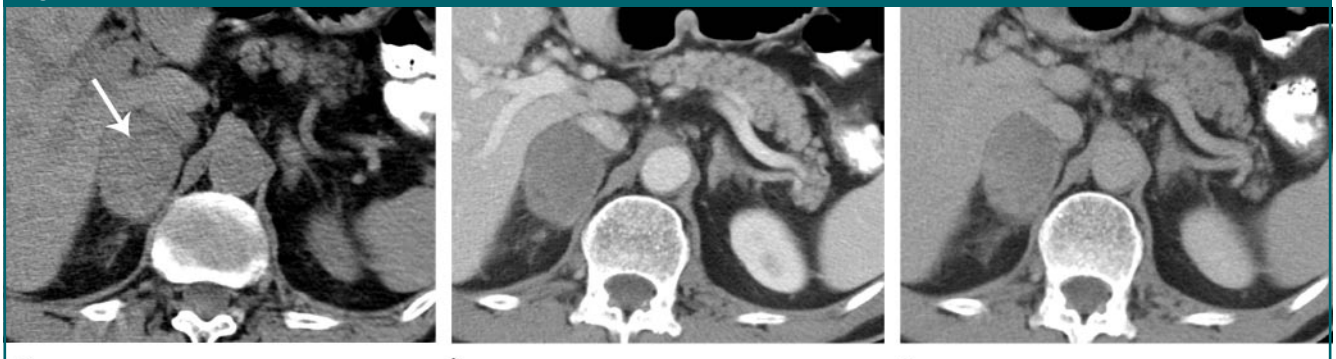

a. b. c.

Figure 10: Axial CT scans of right adrenal metastasis in 71-year-old man with lung cancer. **(a)** Unenhanced scan shows 4.2-cm heterogeneous mass (arrow) with attenuation of 44 HU. **(b)** On dynamic contrast-enhanced scan, mass has attenuation of 73 HU. **(c)** On 15-minute delayed scan, mass has attenuation of 69 HU. APW and RPW are 14% and 5%, respectively, consistent with nonadenoma.

Figure 11

a. b. c.

Figure 11: Axial CT scans of 1.9-cm lipid-poor right adrenal adenoma in 53-year-old woman. **(a)** Unenhanced scan shows adrenal attenuation (arrow) of 16 HU. **(b)** On dynamic contrast-enhanced scan, adrenal attenuation is 53 HU. **(c)** On 15-minute delayed scan, adrenal attenuation is 23 HU. APW and RPW are 81% and 57%, respectively, consistent with lipid-poor adenoma.

out threshold that enables accurate differentiation of adenomas from nonadenomas, most investigators use a 40% threshold on a 15-minute delayed scan for RPW or 60% for APW. Therefore, any lesion that demonstrates RPW > 40% (or APW > 60%) at this time is consistent with an adenoma, with sensitivity and specificity both close to 100%. Lesions that demonstrate RPW < 40% (or APW < 60%) on a 15-minute delayed scan are almost always malignant (Fig 10). Some investigators have recommended using a 10-minute delay scan, because it would be more convenient for busy CT schedules, and setting the RPW threshold at a more conservative 50% (29). Later, other investigators found the 40% RPW threshold to be just as effective even on a 10-minute delayed study (47,49). In practice, however, most investigators still use the 15-minute delayed scan with the 40% RPW threshold.

The sensitivity for differentiating IALs by using RPW is much higher than that achieved with unenhanced CT scans alone. Indeed, it was observed that most lipid-poor adenomas could also be characterized by using this technique, which explains why the test is nearly 100% sensitive and specific (Fig 11) (23,25, 29,45,47). In fact, it has been proposed that RPW (and APW) tests are so effective for differentiating adenomas from nonadenomas that other imaging tests (including MR and PET) should only be needed in unusual circumstances (4,5,45).

Figure 12

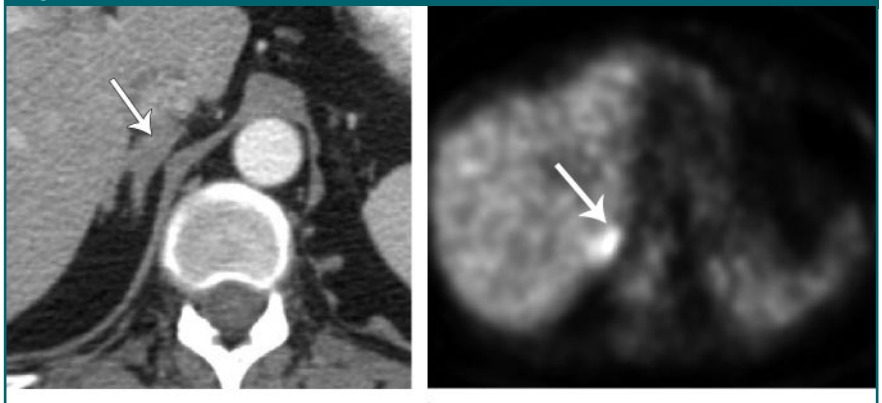

a. b.

Figure 12: Right adrenal metastasis in 64-year-old man with colorectal and renal cell cancer. **(a)** Axial contrast-enhanced CT scan shows slight thickening of right adrenal (arrow). Metastasis was unsuspected. **(b)** Axial PET image shows increased FDG uptake (arrow), strongly suggestive of metastasis, which was confirmed at surgical removal of lesion.

Functional Imaging: PET and PET/CT

Several radioisotopes have been recommended to help characterize IALs including ^{131}I-6-β-iodomethyl-19-norcholesterol (NP-59), MIBG, and fluorine 18 (^{18}F) fluorodeoxyglucose (FDG) PET (50–67). While NP-59 has a high positive predictive value for the detection of adenoma, its widespread use has not been approved by the U.S. Food and Drug Administration, and it effectively has no use in clinical practice. MIBG is still sometimes recommended in the evaluation of some pheochromocytomas, particularly if ectopic or metastatic (53,61,63).

In practice, an increasing number of IALs are now being detected and characterized with PET or PET/CT, as these modalities are now more available. Numerous studies have demonstrated the accuracy of ^{18}F-FDG PET imaging to differentiate benign from malignant adrenal disease (46,50–52,54,56,58,59). Its effi-

cacy works on the principle that ^{18}F-FDG is trapped intracellularly by metabolically active malignant lesions, whereas most benign lesions fail to accumulate the radioisotope (50,53). Hence, very early metastatic disease can be detected by using this technique (Fig 12).

Sensitivity and specificity profiles of PET or PET/CT range from 93% to 100% and 80% to 100%, respectively (46,66,67), although most authors believe that specificity is closer to 95% (56,66). Some adrenal adenomas, adrenal endothelial cysts, and inflammatory and infectious lesions can demonstrate slightly increased radiotracer uptake when compared with the liver (the internal reference organ for normal uptake) (Fig 13). Necrotic or hemorrhagic malignant adrenal lesions may occasionally cause false-negative findings, showing poor ^{18}F-FDG uptake (66). PET is also not recommended for lesions smaller than 1 cm, as metastatic lesions of this size will often demonstrate lower radiotracer uptake than normal liver (66).

PET/CT offers clear advantages over PET alone, because lesion morphology on the CT scan can be coregistered with the metabolic activity on the PET scan on the same image, allowing more accurate anatomic localization of any PET abnormalities (Fig 14). Furthermore, CT densitometry and wash-

Figure 13

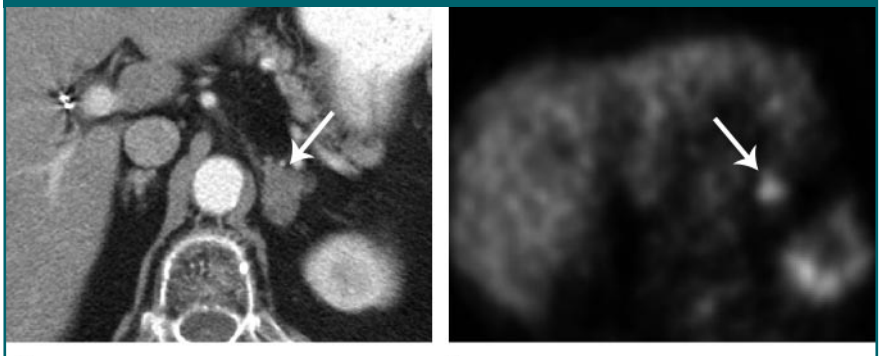

Figure 13: Biopsy-proved left adrenal adenoma in 83-year-old woman with esophageal and lung cancer. **(a)** Axial contrast-enhanced CT scan shows 2.1-cm left adrenal mass (arrow). **(b)** Axial PET image shows slightly increased FDG uptake in adenoma (arrow), as compared with liver.

Figure 14

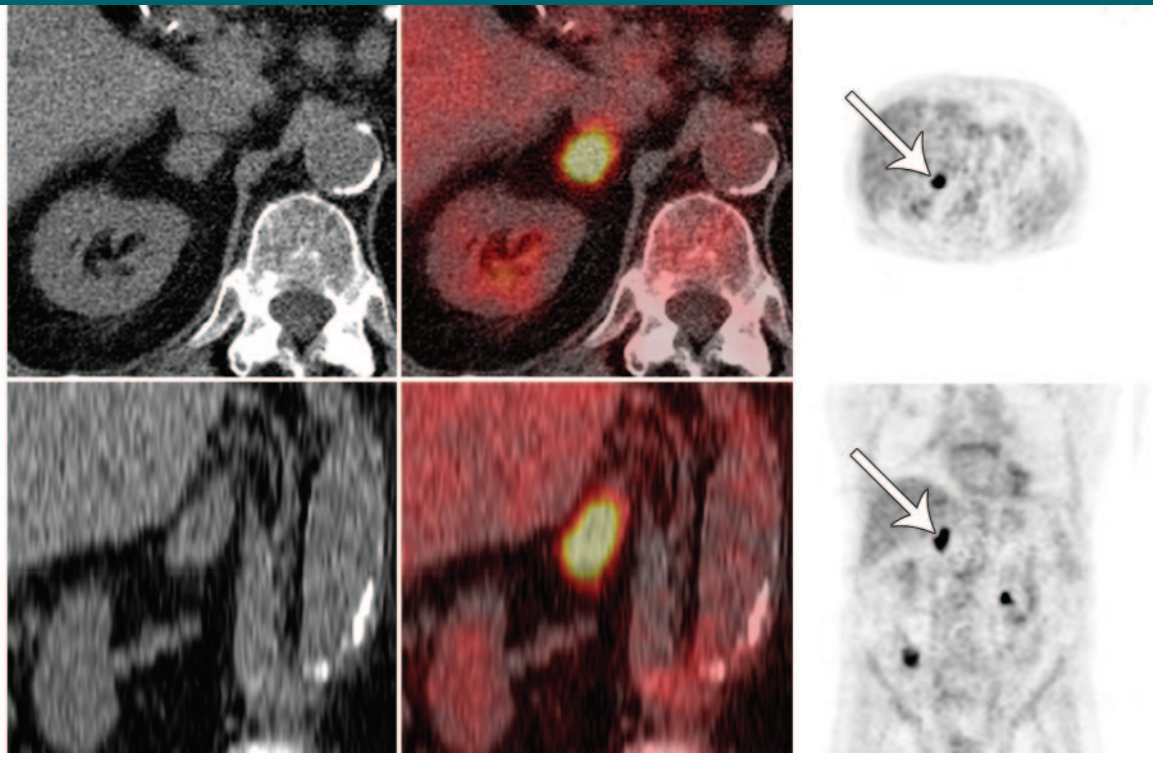

Figure 14: Metastatic lung cancer in 78-year-old woman. Axial (top row) and coronal (bottom row) CT (left column) and PET (right column) images are coregistered (middle column) to show increased FDG uptake (arrows) in 1.4-cm right adrenal metastasis.

Figure 15

Figure 15: Axial contrast-enhanced CT scan in 51-year-old woman with 6-cm right adrenal myelolipoma. Identification of fat (arrow) confirms diagnosis.

Figure 16

a. b.

Figure 16: Lymphoma in 28-year-old woman. **(a)** Axial contrast-enhanced CT scan demonstrates bilateral adrenal masses and necrosis (arrow) in left mass. Washout tests were consistent with nonadenoma. **(b)** Axial PET image shows marked FDG uptake in both masses, with poor uptake in necrotic region (arrow).

out measurements (if contrast-enhanced CT is also performed) can be incorporated into the analysis. Thus, the three most effective tests used to characterize adrenal IALs may be combined into one examination. Under these circumstances, Blake et al (46) demonstrated that the sensitivity and specificity lesion characterization in 41 masses were both 100%, although further studies with larger numbers of patients are required to confirm these findings. In practice, most patients with known IAL will likely be referred for characterization with PET or PET/CT only if CT densitometry or washout analyses are inconclusive on a separate CT study.

Imaging Features of Specific Adrenal Diseases

Cortical Adenoma

Cortical adenoma is the most common adrenal lesion that will be detected at CT and is usually nonfunctioning (Figs 4, 6, 7, 11). Functioning adenomas (Cushing syndrome, Conn syndrome, or adrenogenital hyperplasia) are uncommon and can usually be confirmed by means of biochemical evaluation in the presence of an adrenal mass (1). There are no specific morphologic features that permit adenoma characterization, as most are small, smooth, and homogeneous when detected. However, as discussed, most can be characterized by using lipid-sensitive or washout CT techniques (or sometimes chemical shift MR techniques). If these tests are inconclusive, it is often reasonable to perform follow-up CT at 6 months in a patient who has no history of malignant disease (4,8,68), even if the unenhanced CT adrenal attenuation is greater than 10 HU. A recent study of 973 consecutive patients in this category did not find any malignant lesions at follow-up imaging (9). The chance that an IAL is malignant in this group of patients is therefore negligible.

Metastasis

The adrenal gland is a common site for metastatic disease, most commonly from carcinomas (lung, breast, and colon), lymphoma, and melanoma, although virtually any primary malignancy can metastasize to the adrenal gland (69–71) (Figs 9, 10, 12, 14). Most IALs are, therefore, followed up to diagnosis in patients with a known extraadrenal malignancy (1). The primary malignancy is usually known at time of diagnosis, and lesion characterization is critical for primary disease staging and treatment planning (1). Similar to most adenomas, metastases do not usually demonstrate specific morphologic imaging features, unless they have increased in size on serial images or are large, irregular, and/or necrotic. Not infrequently, they can be bilateral. Rarely, a metastasis can occur in an existing adenoma, which is then known as a "collision" tumor. In the setting of a known primary extraadrenal malignancy, a lesion on CT washout images that does not conform to strict criteria for benignity should be strongly considered as metastatic.

Myelolipoma

Myelolipomas are usually detected incidentally at CT, and although most are small, they can occasionally be large, hemorrhagic, or, rarely, extraadrenal (4,14,15,72). Most, however, have specific imaging features that permit easy characterization with CT or MR imaging due to their abundance of mature fat (Fig 7). The amount of recognizable macroscopic fat varies from almost 100% to none. However, the presence of even the slightest macroscopic fat indicates that the lesion is a myelolipoma (Fig 15). Calcification can also be identified in approximately 20% of cases (39). When a myelolipoma is large (>5 cm), the myeloid elements have a tendency to hemorrhage. For these reasons, some larger myelolipomas are surgically removed.

While CT can enable characterization of almost all lesions, MR imaging can oc-

casionally be helpful by demonstrating high fat signal intensity on T1- and T2-weighted images, which is reduced on fat-suppression images. Chemical shift imaging may or may not be helpful, depending on the proportion of fat to water in an MR imaging voxel, since pure fat may demonstrate no signal intensity decrease on opposed-phase images (Fig 7).

Lymphoma

Primary adrenal lymphoma is extremely rare, but metastatic involvement is more common, with approximately 4% of patients with non-Hodgkin lymphoma demonstrating adrenal involvement (1,3,73,74) (Fig 16). Imaging features include total encasement of the adrenal gland from adjacent retroperitoneal disease (making it hard to identify the adrenal gland) to smaller discrete masses or diffuse enlargement. Bilateral metastatic involvement occurs in up to 50% of cases (8,73). Lymphoma-related lesions demonstrate washout characteristics similar to those of other malignancies and may demonstrate heterogeneous hyperintensity on T2-weighted MR images, but this

Figure 17

Figure 17: Axial CT scans in 31-year-old woman with 11.8-cm right adrenal carcinoma. **(a)** Unenhanced scan shows mass with necrosis (long arrow) and calcification (short thin arrow). Attenuation in circular ROI in solid soft-tissue area of mass (thick arrow) is 40 HU. **(b)** On dynamic contrast-enhanced scan, attenuation is 81 HU in solid area of mass. **(c)** On 15-minute delayed contrast-enhanced scan, attenuation is 70 HU in solid area of mass. APW and RPW of 27% and 14%, respectively, are consistent with malignancy.

Figure 18

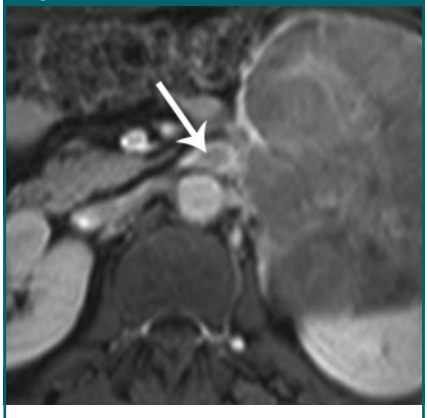

Figure 18: Axial gadolinium-enhanced T1-weighted three-dimensional gradient-echo MR image (5.5/1.7, 15° flip angle) in 61-year-old woman with 10.3-cm left adrenal carcinoma shows invasion by tumor of left adrenal and renal veins (arrow).

Figure 19

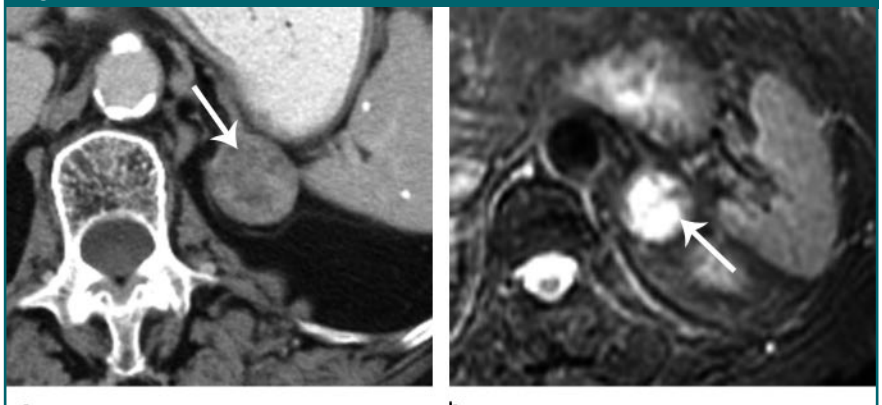

Figure 19: Left adrenal pheochromocytoma in 67-year-old woman. **(a)** Axial contrast-enhanced CT scan shows 2.9-cm indeterminate mass (arrow). Mass is heterogeneous, with attenuation of 66 HU. **(b)** Axial T2-weighted fast spin-echo MR image (4000/100, 90° flip angle) shows hyperintense signal (arrow), suggestive of pheochromocytoma.

finding is nonspecific (4,8,46). PET usually demonstrates increased radionuclide uptake, but uptake can rapidly decrease after the use of appropriate chemotherapy (56,66).

Adrenal Carcinoma

Adrenal carcinoma is rare, and most lesions are larger than 6 cm when detected, despite the fact that 50% of patients present with Cushing syndrome (from cortisol hypersecretion) or, more rarely, Conn syndrome or adrenogenital syndrome (16,75–78). Lesions are typically heterogeneous and irregular, and calcification is seen in up to 30% of cases (75,76). Lesions enhance heterogeneously after intravenous administration of contrast material and demonstrate CT washout values consistent with those of other malignant diseases (Fig 17) (16). Important surgical considerations involve determining the cephalad extension of large tumors or invasion of adjacent vascular structures (Fig 18). Multiplanar imaging with MR or multidetector CT can be helpful in these circumstances.

Pheochromocytoma

Pheochromocytoma, a rare catecholamine-secreting tumor, usually manifests clinically, but up to 10% are detected incidentally (10,16,79–81) (Figs 19, 20). Another 10% are also bilateral or extraadrenal in location (along the paraganglionic sympathetic nervous system) or malignant (82).

The diagnosis of pheochromocytoma is dependent on detection of an adrenal mass in the appropriate clinical and biochemical setting. Imaging appearances are variable. At CT, most lesions are smooth and round, with attenuation similar to that of soft tissue. They avidly enhance after intravenous administration of contrast medium, and washout characteristics are typically similar to those malignant adrenal lesions, regardless of whether the pheochromocytoma is malignant or benign (16). However, uncommonly, pheochromocytoma may show the opposite, with washout values consistent with benign disease, low attenuation at unenhanced CT, or poor enhancement after intravenous administration of contrast medium (16,82,83). Macroscopic fat can even be identified on rare occasions (83,84). Because pheochromocytoma can be confused with an adenoma on rare occasions, some endocrinologists recommend biochemical evaluation for any patient suspected of having an adenoma on the basis of imaging findings (1). Large lesions are often heterogeneous and necrotic and are usually nonfunctioning (85).

Traditionally, it had been thought that the use of intravenous iodinated contrast medium at CT could precipitate a hypertensive crisis in patients with pheochromocytoma. However, several reports have now documented that the use of intravenous nonionic contrast medium poses no markedly increased risk when evaluating patients with CT (86–88).

Up to 70% lesions demonstrate high signal intensity on T2-weighted MR images; this finding is thought to be somewhat characteristic of pheochromocy-

Figure 20

a. b.

Figure 20: Recurrent metastatic pheochromocytoma in 48-year-old man. **(a)** Axial contrast-enhanced CT scan shows 6-cm recurrence (arrow) in upper pelvis. **(b)** Anteroposterior MIBG image shows increased radiotracer uptake (arrow) in upper pelvis, consistent with recurrent pheochromocytoma.

Figure 21

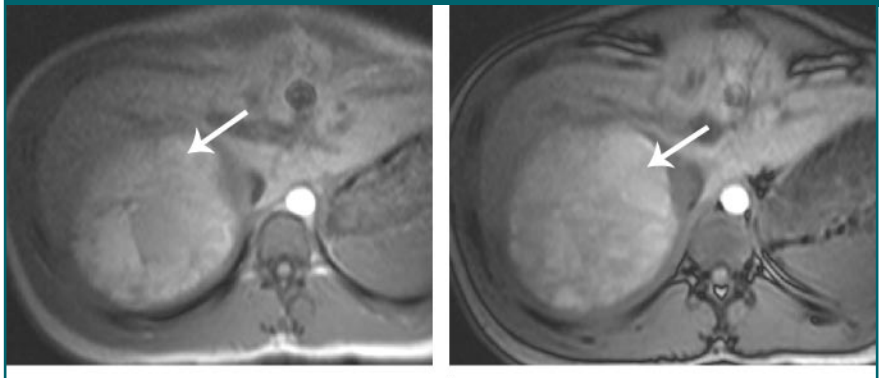

a. b.

Figure 21: Axial MR images of adrenal hemorrhage in 24-year-old woman. **(a)** T1-weighted gradient-echo in-phase image (180/4.2, 80° flip angle) shows 12-cm right adrenal mass (arrow) with mixed signal intensity. **(b)** T1-weighted gradient-echo opposed-phase image (180/2.1, 80° flip angle) shows that predominantly high adrenal signal intensity remains (arrow), confirming areas consistent with hemorrhage.

toma and can also be used to help characterize extraadrenal disease (Fig 19) (8,82,85). However, 30% of lesions demonstrate low signal intensity on T2-weighted images and may be confused with other adrenal disease (8,82).

MIBG scintigraphy can play a role in problem cases. Iodine 123– or iodine 131–labeled MIBG is concentrated within pheochromocytomas, and its use has proved particularly helpful in patients with strong biochemical evidence of tumor but no CT evidence of disease or for confirmation of extraadrenal or metastatic disease (Fig 20) (53,61,63, 64,82,89). MIBG has almost 100% specificity for the diagnosis of pheochromocytoma, but its sensitivity is variable (53,89). Octreotide, a somatostatin analog, can occasionally be helpful but has only 30% sensitivity (90). However, with the increasing availability of PET, MIBG imaging is less often performed for this disease (53,62,91). Imaging with 6-[^{18}F]fluorodopamine and carbon 11–hydroxyephedrine PET has also shown promising initial results for detection and characterization of pheochromocytoma (92,93).

Hemorrhage

Blunt trauma accounts for 80% of adrenal hemorrhages, which are usually uni-

Figure 22

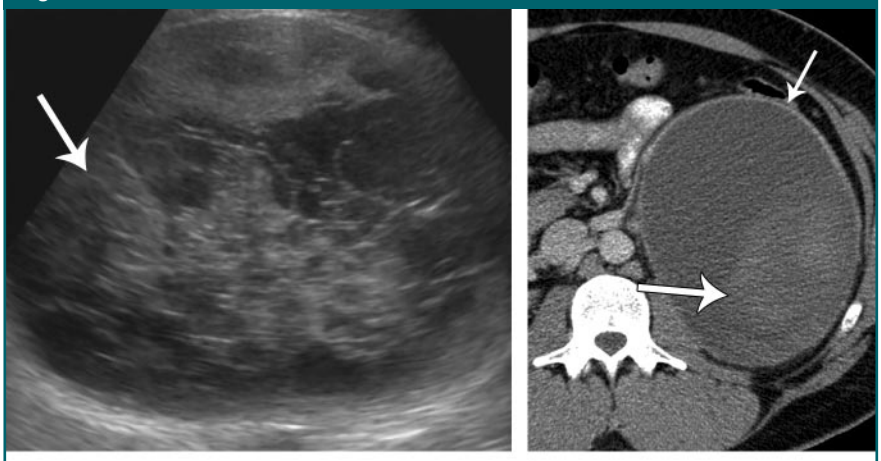

a. b.

Figure 22: A 17-cm left adrenal cyst in 43-year-old woman. **(a)** Sagittal US image of mass shows complex cyst with marked internal echoes (arrow). **(b)** Axial contrast-enhanced CT scan shows slightly thickened wall (short arrow) and cyst with mixed components (long arrow). Owing to cyst's complex nature, percutaneous biopsy was performed to exclude cystic neoplasm; results confirmed benign adrenal cyst.

Figure 23

Figure 23: Coronal T1-weighted three-dimensional gradient-echo MR image (5.5/1.7, 15° flip angle) in 24-year-old woman with neuroblastoma shows 16-cm complex right adrenal mass (arrow) with necrosis and hemorrhage. (Image courtesy of Nagaraj Holakere, MD.)

Figure 24

Figure 24: Axial contrast-enhanced CT scan shows homogeneous 6-cm left adrenal mass (arrow) in 55-year-old woman. Adrenal biopsy yielded ganglioneuroma.

Figure 25

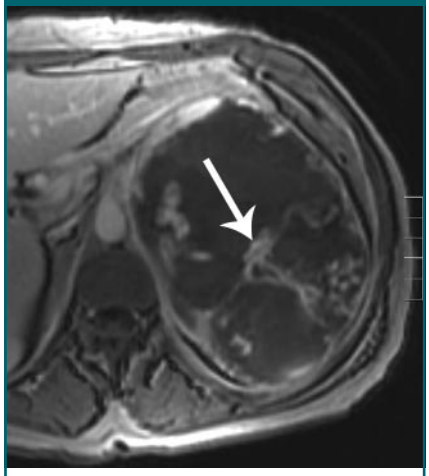

Figure 25: Axial gadolinium-enhanced T1-weighted gradient-echo MR image (180/2.1, 80° flip angle) in 53-year-old woman with hemangiosarcoma shows 14-cm left adrenal mass with marked vascularity (arrow).

Figure 26

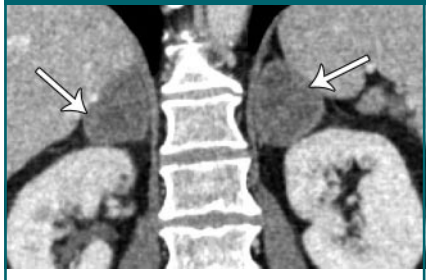

Figure 26: Coronal contrast-enhanced CT scan in 60-year-old man with histoplasmosis shows bilateral uniform homogeneous adrenal masses (arrows). Left and right adrenal glands measure 5.2 and 4.9 cm in the coronal plane, respectively. (Image courtesy of Mukesh Harisinghani, MD.)

Figure 27

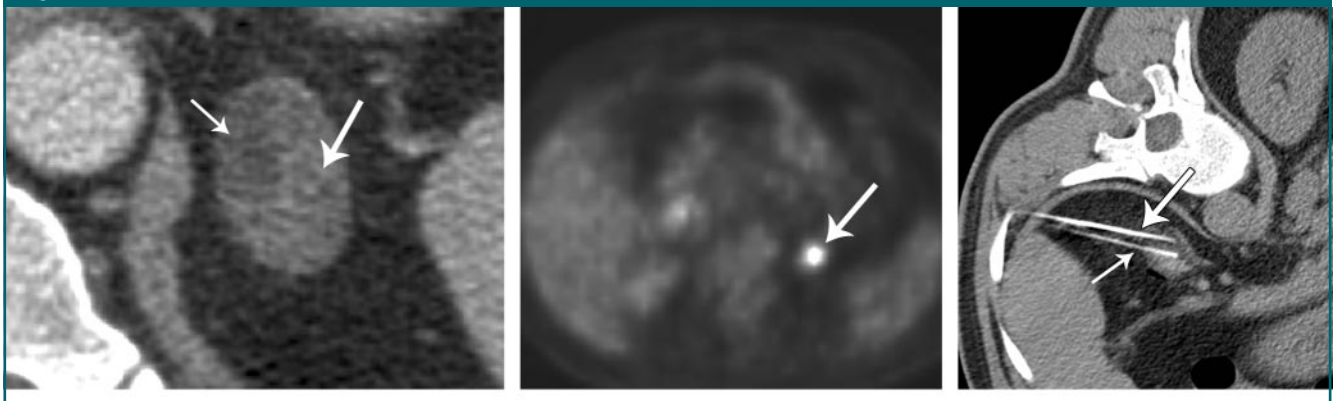

a. b. c.

Figure 27: Previously known left adrenal adenoma, and new "collision" tumor (leiomyosarcoma) to inferior aspect of mass in 50-year-old man. **(a)** Axial unenhanced CT scan shows 2.6-cm left adrenal mass with new areas of higher attenuation in lateral and inferior aspects of previously uniform hypoattenuating mass (long arrow). Areas of lower attenuation are seen medially (short arrow). **(b)** Axial PET image shows marked FDG uptake (arrow) in inferior aspect of mass, strongly suggestive of metastatic disease. **(c)** Axial unenhanced CT scan during left adrenal biopsy with patient in left lateral decubitus position. Specimen obtained with medial needle (long arrow) confirmed adenoma; specimen from lateral needle (short arrow) confirmed metastasis.

Figure 28

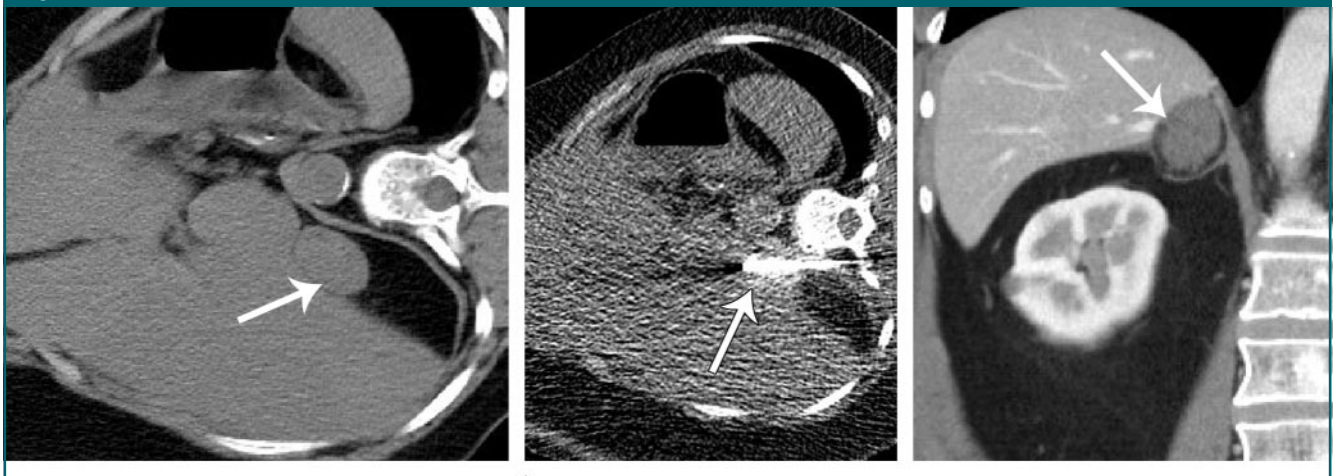

a. b. c.

Figure 28: CT scans in 54-year-old woman referred for right adrenal percutaneous radiofrequency ablation. Patient had previously undergone left nephrectomy for renal cell carcinoma, and new biopsy findings proved the presence of right adrenal metastasis. Patient was not a surgical candidate owing to severe coronary artery disease and systemic lupus erythematosus. **(a)** Immediate preablation axial unenhanced scan with patient in right lateral decubitus position shows 2.5-cm right adrenal metastasis (arrow). **(b)** Axial unenhanced scan with patient in right lateral decubitus position shows radiofrequency needle in the mass (arrow). **(c)** Coronal contrast-enhanced scan 2.5 years after ablation shows that mass is stable and demonstrates no evidence of progression.

lateral and are more common on the right (94) (Fig 21). When bilateral, hemorrhage is usually associated with bleeding diatheses or severe stress (95). Adrenal hemorrhage has also been reported after adrenal venous sampling for endocrine disease (96,97). If spontaneous, an underlying adrenal tumor should be considered, and follow-up imaging or biopsy is required.

Acute adrenal hemorrhage will show increased CT attenuation of 50–90 HU on unenhanced CT scans, which slowly decreases over time, as does the size of the mass. In the acute setting, if a contrast-enhanced study is performed, it can be difficult to distinguish from other indeterminate adrenal masses, and follow-up imaging is required (4). MR appearances include hyperintensity (methemoglobin) on T1-weighted images, seen in subacute

hemorrhage, or a dark rim on T2-weighted images when hemorrhage is chronic (8).

Cyst

These are uncommon lesions resulting from endothelial proliferation, prior hemorrhage, or parasitic disease (85,98). They usually demonstrate the expected cystic CT and MR imaging features but some have higher attenuation values at CT (8,99). They usually have thin (<3-mm-thick) walls and may contain internal septa, both of which can enhance or contain calcifications (Fig 22) (17). The only noteworthy diagnostic challenge is to ensure that the lesion is not a cystic adrenal adenocarcinoma, although such lesions are almost never purely cystic (17).

Neuroblastoma

Neuroblastoma can occasionally be seen in adults, although it is a tumor usually associated with childhood (Fig 23). It is found anywhere along the sympathetic nervous system chain. Adults typically show less calcification but more metastatic disease than do children (100,101). In adults, the findings are hard to differentiate from other malignant diseases, and biopsy is usually required.

Ganglioneuroma

Ganglioneuroma is a rare benign tumor that is usually detected incidentally (4) (Fig 24). Although it can arise in the adrenal medulla, most are extraadrenal, located along the paravertebral sympathetic plexus (102,103). These tumors can be very large (>20 cm), and there are no specific imaging features, although even large masses show homogeneous or mildly heterogeneous enhancement, which is unusual for a mass of this size (4).

Hemangioma and Hemangiosarcoma

Adrenal hemangioma is a rare tumor and is usually benign, except for the even rarer hemangiosarcoma (104). They are often very large when detected, owing to their indolent nature, and are highly vascular, demonstrating irregular and profuse enhancement (Fig 25). Specific features include the presence of multiple phleboliths within the tumor and persistent enhancement on delayed images (105,106). On MR images, these tumors are usually hyperintense on T2-weighted images and hypointense on T1-weighted images.

Granulomatous Disease

Worldwide, tuberculous adrenal disease occurs much more commonly than histoplasmosis and blastomycosis (Fig 26). However, the imaging findings are similar in each disease: usually bilateral homogeneous adrenal enlargement when acute and sometimes cystic or calcified when chronic (107–109). Tuberculous adrenal atrophy can also occur in chronic disease, leading to adrenal hypofunction and Addison disease (108).

Figure 29

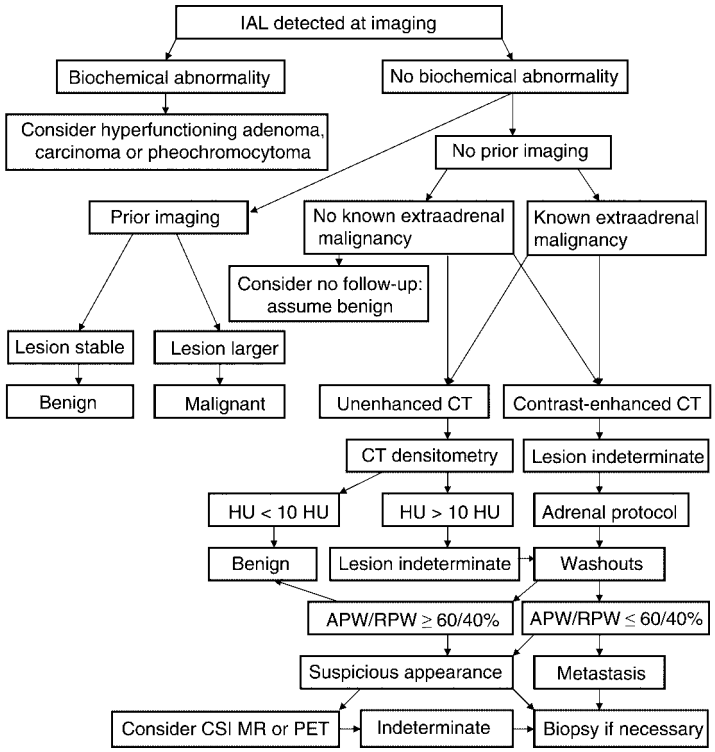

Figure 29: Flowchart shows algorithmic approach to characterization of IAL detected at CT.

Adrenal Interventional Techniques: Adrenal Biopsy and Ablation

Adrenal Biopsy

The necessity for adrenal biopsy has been reduced by the accuracy of contemporary adrenal imaging techniques designed to characterize adrenal disease (110) (Fig 27). Biopsy is still recommended in select cases, however, particularly if the patient has an underlying extraadrenal malignancy. Sometimes, findings from conventional adrenal imaging are inconclusive or there is suspicion that the lesion could still be malignant, despite imaging evidence to the contrary (eg, lesion stability on serial images, inconsistent washout results, PET findings suggestive of malignancy). The frequency of and necessity for adrenal biopsy will likely depend on a department's familiarity with adrenal imaging and biopsy techniques.

Adrenal biopsy procedures are generally safe, with a low complication rate (most commonly, adrenal hemorrhage or pneumothorax), and accurate (83%–96% diagnostic accuracy) (110–112). Approximately 50%–70% of those pa-

tients' biopsies will yield benign disease, even in patients with malignancy (112). Biopsy is not generally indicated for patients suspected of having pheochromocytoma, owing to the risk of precipitating a hypertensive crisis, although these tumors have sometimes been inadvertently subjected to biopsy without untoward clinical complications (111,112).

The biopsy procedure is usually performed with CT guidance while the patient is in the decubitus position with the adrenal mass ipsilateral side down to reduce the risk of pneumothorax (Fig 27). Rarely, it may be necessary to use a transhepatic approach (8).

Adrenal Ablation

Radiofrequency ablation is a technique that uses alternating current to generate heat and induce tissue necrosis (113–115). It involves placement of radiofrequency electrodes into the tumor by using a technique similar to adrenal biopsy; the complication rate has been reported to be low (113,114). A variety of adrenal tumors have been treated, including metastatic disease (Fig 28), pheochromocytoma, aldosteronoma, and recurrent adrenal carcinoma (113,116). Proper patient selection is critical and is usually indicated for those patients with an extraadrenal primary cancer with no other evidence of metastatic disease or controlled disease at other sites (113). Because follow-up imaging has often helped identify progressive extraadrenal metastatic disease, the technique is usually reserved for palliative purposes. However, radiofrequency ablation could play a more definitive role for the treatment of hyperfunctioning adrenal neoplasms (113).

Differentiation of Adenoma from Malignant Adrenal Disease: Imaging Algorithm

While there are numerous lesions that can potentially affect the adrenal gland, the most common clinical challenge is to differentiate a metastasis from an adenoma in a patient with an extraadrenal malignancy. Ideally, a previous abdominal or chest CT study is available for comparison, but other studies such as a spine MR imaging or renal MR angiographic study can also prove effective. Lesion stability at 6 months almost always signifies benignity.

If no prior imaging study is available or is inconclusive, an adrenal CT protocol is recommended involving an initial unenhanced study followed by CT washout studies. Almost all lesions can be differentiated into benign or malignant (or at least highly suspicious for malignancy) categories with these techniques. Diagnosis of the few remaining uncharacterized lesions might occasionally benefit from chemical shift MR or PET imaging. Alternatively, adrenal biopsy can be performed for these few remaining cases where a timely diagnosis is critical. Otherwise 6-month follow-up imaging is a reasonable approach, although some radiologists recommend an earlier 4-month follow-up in patients with malignant disease if biopsy is not performed. Finally, because an IAL is very unlikely to represent metastatic disease in patients without a known extraadrenal malignancy, some referring physicians prefer no imaging follow-up (once they have excluded functioning disease), assuming the lesion to be a nonfunctioning adenoma. The algorithm shown in Figure 29 is suggested when attempting to characterize an IAL.

References

1. Young WF Jr. The incidentally discovered adrenal mass. N Engl J Med 2007;356:601–610.
2. Bovio S, Cataldi A, Reimondo G, et al. Prevalence of adrenal incidentaloma in a contemporary computerized tomography series. J Endocrinol Invest 2006;29:298–302.
3. Mansmann G, Lau J, Blak E, et al. The clinically inapparent adrenal mass: update in diagnosis and treatment. Endocr Rev 2004;25:309–340.
4. Dunnick NR, Korobkin M. Imaging of adrenal incidentalmomas. AJR Am J Roentgenol 2002;179:559–568.
5. Korobkin M. CT characterization of adrenal masses: the time has come. Radiology 2000;217:629–632.
6. Kloos RT, Gross MD, Francis IR, et al. Incidentally discovered adrenal masses. Endocr Rev 1995;16:460–484.
7. Young WF Jr. Management approaches to adrenal incidentalomas: a view from Rochester, Minnesota. Endocrinol Metab Clin North Am 2000;29:159–185.
8. Mayo-Smith WW, Boland GW, Noto RB, et al. State-of-the-art adrenal imaging. RadioGraphics 2001;21:995–1012.
9. Song JH, Chaudhry FS, Mayo-Smith WW. The incidental indeterminate adrenal mass on CT: prevalence of adrenal disease in 1,049 consecutive adrenal masses in patients with no known malignancy. AJR Am J Roentgenol 2008;190:1163–1168.
10. Slattery JM, Blake MA, Kalra MK, et al. Adrenocortical carcinoma: contrast washout characteristics on CT. AJR Am J Roentgenol 2006;187:W21–W24.
11. Angeli A, Osella G, Ali A, et al. Adrenal incidentaloma: an overview of clinical and epidemiological data from the National Italian Study Group. Horm Res 1997;47:279–283.
12. Abrams HL, Spiro R, Goldstein N. Metastases in carcinoma: analysis of 1000 autopsied cases. Cancer 1950;3:74–85.
13. Boland GW, Lee MJ, Gazelle GS, et al. Characterization of adrenal masses using unenhanced CT: an analysis of the CT literature. AJR Am J Roentgenol 1998;171:201–204.
14. Goldman HB, Howard RC, Patterson AL. Spontaneous retroperitoneal hemorrhage from a giant adrenal myelolipoma [letter]. J Urol 1996;155:639.
15. Russell C, Goodacre BW, vanSonnenberg E, Orihuela E. Spontaneous rupture of adrenal myelolipoma: spiral CT appearance. Abdom Imaging 2000;25:431–434.
16. Szolar DH, Melvyn Korobkin M, Reittner P, et al. Adrenocortical carcinomas and adrenal pheochromocytomas: mass and enhancement loss evaluation at delayed contrast-enhanced CT. Radiology 2005;234:479–485.
17. Rozenblit A, Morehouse HT, Amis SE Jr. Cystic adrenal lesions: CT features. Radiology 1996;201:541–548.
18. Benitah N, Yeh BM, Qayyum A. Minor morphologic abnormalities of adrenal glands at CT: prognostic importance in patients with lung cancer. Radiology 2005;235:517–522.
19. Korobkin M, Giordano TJ, Brodeur FJ, et al. Adrenal adenomas: relationship between histologic lipid and CT and MR findings. Radiology 1996;200:743–747.
20. Anderson JB, Gray GF. Adrenal pathology. In: Vaughan ED, Carey RM, eds. Adrenal

disorders. New York, NY: Thieme Medical, 1989; 18–19.

21. Carney JA. Adrenal gland. In: Sternberg SS, ed. Histology for pathologists. New York, NY: Raven, 1992; 150–154.
22. Lee MJ, Hahn PF, Papanicolau N, et al. Benign and malignant adrenal masses: CT distinction with attenuation coefficients, size, and observer analysis. Radiology 1991;179:415–418.
23. Caoili EM, Korobkin M, Francis IR, et al. Adrenal masses: characterization with combined unenhanced and delayed enhanced CT. Radiology 2002;222:629–633.
24. Hahn PF, Blake MA, Boland GW. Adrenal lesions: attenuation measurement differences between CT scanners. Radiology 2006;240:458–463.
25. Caoili EM, Korobkin M, Francis IR, Cohan RH, Dunnick NR. Delayed enhanced CT of lipid-poor adrenal adenomas. AJR Am J Roentgenol 2000;175:1411–1415.
26. Korobkin M, Brodeur FJ, Yutzy GG, et al. Differentiation of adrenal adenomas from nonadenomas using CT attenuation values. AJR Am J Roentgenol 1996;166:531–536.
27. Korobkin M, Brodeur FJ, Francis IR, Quint LE, Dunnick NR, Londy F. CT time-attenuation washout curves of adrenal adenomas and nonadenomas. AJR Am J Roentgenol 1998;170:747–752.
28. Szolar DH, Kammerhuber FH. Adrenal adenomas and nonadenomas: assessment of washout at delayed contrast-enhanced CT. Radiology 1998;207:369–375.
29. Pena CS, Boland GW, Hahn PF, Lee MJ, Mueller PR. Characterization of indeterminate (lipid-poor) adrenal masses: use of washout characteristics at contrast-enhanced CT. Radiology 2000;217:798–802.
30. Boland GW, Hahn PF, Pena C, Mueller PR. Adrenal masses: characterization with delayed contrast-enhanced CT. Radiology 1997;202:693–696.
31. Bae KT, Fuangtharnthip P, Prasad SR, Joe BN, Heiken JP. Adrenal masses: CT characterization with histogram analysis method. Radiology 2003;228:735–742.
32. Jhaveri KS, Wong F, Ghai S, Haider MA. Comparison of CT histogram analysis and chemical shift MRI in the characterization of indeterminate adrenal nodules. AJR Am J Roentgenol 2006;187:1303–1308.
33. Remer EM, Motta-Ramirez GA, Shepardson LB, Hamrahian AH, Herts BR. CT histogram analysis in pathologically proven adrenal masses. AJR Am J Roentgenol 2006;187:191–196.
34. Mitchell DG, Crovello M, Matteucci T, Peterson RO, Miettinen MM. Benign adrenocortical masses: diagnosis with chemical shift MR imaging. Radiology 1992;185:345–351.
35. Reinig JW, Stutley JE, Leonhurdt CM, Spicer KM, Margolis M, Caldwell CB. Differentiation of adrenal masses with MR imaging: comparison of techniques. Radiology 1994;192:41–46.
36. Outwater EK, Siegelman ES, Radecki PD, Piccoli CW, Mitchell DG. Distinction between benign and malignant adrenal masses: value of T1-weighted chemical-shift MR imaging. AJR Am J Roentgenol 1995;165:579–583.
37. Korobkin M, Lombardi TJ, Aisen AM, et al. Characterization of adrenal masses with chemical shift and gadolinium-enhanced MR imaging. Radiology 1995;197:411–418.
38. Outwater EK, Siegelman ES, Huang AB, Birnbaum BA. Adrenal masses: correlation between CT attenuation value and chemical shift ratio at MR imaging with in-phase and opposed-phase sequences. Radiology 1996; 200:749–752.
39. Rao P, Kenney PJ, Wagner BJ, Davidson AJ. Imaging and pathologic features of myelolipoma. RadioGraphics 1997;17:1373–1385.
40. Fujiyoshi F, Nakajo M, Kukukura Y, Tsuchimochi S. Characterization of adrenal tumors by chemical shift fast-low angle shot MR imaging: comparison of four methods of quantitative evaluation. AJR Am J Roentgenol 2003;180:1649–1657.
41. Mayo-Smith WW, Lee MJ, McNicholas MM, Hahn PF, Boland GW, Saini S. Characterization of adrenal masses (<5 cm) by use of chemical shift MR imaging: observer performance versus quantitative measures. AJR Am J Roentgenol 1995;165:91–95.
42. McNicholas MM, Lee MJ, Mayo-Smith WW, Hahn PF, Boland GW. Mueller PR. An imaging algorithm for the differential diagnosis of adrenal adenomas and metastases. AJR Am J Roentgenol 1995;165: 1453–1459.
43. Israel GM, Korobkin M, Wang C, Hecht EN, Krinsky GA. Comparison of unenhanced CT and chemical shift MRI in evaluating lipid-rich adrenal adenomas. AJR Am J Roentgenol 2004;183:215–219.
44. Haider MA, Ghai S, Jhaveri K, Lockwood G. Chemical shift MR imaging of hyperattenuating (>10 HU) adrenal masses: does it still have a role? Radiology 2004;231:711–716.
45. Park BK, Kim CK, Kim B, Lee JH. Comparison of delayed enhanced CT and chemical shift MR for evaluating hyperattenuating incidental adrenal masses. Radiology 2007; 243:760–765.
46. Blake MA, Slattery JM, Kalra MK, et al. Adrenal lesions: characterization with fused PET/CT image in patients with proved or suspected malignancy—initial experience. Radiology 2006;238:970–977.
47. Blake MA, Kalra MK, Sweeney AT, et al. Distinguishing benign from malignant adrenal masses: multi-detector row CT protocol with 10-minute delay. Radiology 2005;238: 578–585.
48. Krestin GP, Steinbrich W, Friedmann G. Adrenal masses: evaluation with fast gradient-echo MR imaging and Gd-DTPA-enhanced dynamic studies. Radiology 1989; 171:675–680.
49. Fogel J, Blake MA, Kalra MK, et al. A 10-minute CT protocol for differentiating benign from malignant adrenal masses [letter]. Radiology 2007;242:947–948.
50. Maurea S, Mainolfi C, Bazzicalupo I, et al. Imaging of adrenal tumors using FDG-PET: comparison of benign and malignant lesions. AJR Am J Roentgenol 1999;173: 25–29.
51. Boland GW, Goldberg MA, Lee MJ, et al. Indeterminate adrenal mass in patients with cancer: evaluation at PET with 2-[F-18]-fluoro-2-deoxy-D-glucose. Radiology 1995;194:131–134.
52. Erasmus JJ, Patz EF Jr, McAdams HP, et al. Evaluation of adrenal masses in patients with bronchogenic carcinoma using ^{18}F-fluorodeoxyglucose positron emission tomography. AJR Am J Roentgenol 1997; 168:1357–1360.
53. Maurea S, Klain M, Mainolfi C, Ziviello M, Salvatore M. The diagnostic role of radionuclide imaging in evaluation of patients with nonhypersecreting adrenal masses. J Nucl Med 2001;42:884–892.
54. Gupta NC, Graeber GM, Tamim WJ, Rogers JS, Irisari L, Bishop HA. Clinical utility of PET-FDG imaging in differentiation of benign from malignant adrenal masses in lung cancer. Clin Lung Cancer 2001;3:59–64.
55. Rohren EM, Turkington TG, Coleman RE. Clinical applications of PET in oncology. Radiology 2004;231:305–332.
56. Elaini AB, Shetty SK, Chapman VM, et al. Improved detection and characterization of adrenal disease with PET-CT. RadioGraphics 2007; 27:755–767.
57. Metser U, Miller E, Lerman H, Lievshitz G, Avital S, Even-Sapir E. ^{18}F-FDG PET/CT in

the evaluation of adrenal masses. J Nucl Med 2006;47:32–37.

58. Rao SK, Caride VJ, Ponn R, Giakovis E, Lee SH. F-18 fluorodeoxyglucose positron emission tomography-positive benign adrenal cortical adenoma: imaging features and pathologic correlation. Clin Nucl Med 2004; 29:300–302.

59. Bagheri B, Maurer AH, Cone L, Doss M, Adler L. Characterization of the normal adrenal gland with ^{18}F-FDG PET/CT. J Nucl Med 2004;45:1340–1343.

60. Francis IR, Smid A, Gross MD, et al. Adrenal masses in oncologic patients: functional and morphologic evaluation. Radiology 1988;166:353–356.

61. Francis IR, Glazer GM, Shapiro B, Sisson JC, Gross BH. Complementary roles of CT and ^{131}I-MIBG scintigraphy in diagnosing pheochromocytoma. AJR Am J Roentgenol 1983;141:719–725.

62. Shulkin BL, Koeppe RA, Francis IR, Deeb GM, Lloyd RV, Thompson NW. Pheochromocytomas that do not accumulate metaiodobenzylguanidine: localization with PET and administration of FDG. Radiology 1993;186:711–715.

63. Shapiro B, Copp JE, Sisson JC, Eyre PL, Wallis J, Beierwaltes WH. Iodine-131 metaiodobenzylguanidine for the locating of suspected pheochromocytoma: experience in 400 cases. J Nucl Med 1985;26:576–585.

64. Maurea S, Cuocolo A, Reynolds JC, et al. Iodine-131-metaiodobenzylguanidine scintigraphy in preoperative and postoperative evaluation of paragangliomas: comparison with CT and MRI. J Nucl Med 1993;34: 173–179.

65. Freitas JE. Adrenal cortical and medullary imaging. Semin Nucl Med 1995;25:235–250.

66. Chong S, Lee KS, Kim AH. Integrated PET-CT for the characterization of adrenal lesions in cancer patients: diagnostic efficacy and interpretation pitfalls. RadioGraphics 2006;26:1811–1826.

67. Yun M, Kim W, Alnafisi N, Lacorte L, Jang S, Alavi A. ^{18}F-FDG PET in characterizing adrenal lesions detected on CT or MRI. J Nucl Med 2001;42:1795–1799.

68. Lee JE, Evans DB, Hickey RC, et al. Unknown primary cancer presenting as an adrenal mass: frequency and implications for diagnostic evaluation of adrenal incidentalomas. Surgery 1998;124:1115–1122.

69. Lenert JT, Barnett CC Jr, Kudelka AP, et al. Evaluation and surgical resection of adrenal masses in patients with a history of extra-adrenal malignancy. Surgery 2001; 130:1060–1067.

70. Zornoza J, Bracken R, Wallace S. Radiologic features of adrenal metastases. Urology 1976;8:295–299.

71. Lam KY, Lo CY. Metastatic tumors of the adrenal glands: a 30-year experience in a teaching hospital. Clin Endocrinol (Oxf) 2002;56:95–101.

72. Kumar M, Duerinckx AJ. Bilateral extraadrenal perirenal myelolipoma: an imaging challenge. AJR Am J Roentgenol 2004;183: 833–836.

73. Paling MR, Williamson BR. Adrenal involvement in non-Hodgkin lymphoma. AJR Am J Roentgenol 1983;141:303–305.

74. Glazer HS, Lee JK, Balfe DM, Mauro MA, Griffith R, Sagel SS. Non-Hodgkin lymphoma: computed tomographic demonstration of unusual extranodal involvement. Radiology 1983; 149:211–217.

75. Dunnick NR, Heaston D, Halvorsen R, Moore AV, Korobkin M. CT appearance of adrenal cortical carcinoma. J Comput Assist Tomogr 1982;6:978–998.

76. Fishman EK, Deutch BM, Hartman DS, Goldman SM, Zerhouni EA, Siegelman SS. Primary adrenocortical carcinoma: CT evaluation with clinical correlation. AJR Am J Roentgenol 1987;148:531–535.

77. Copeland PM. The incidentally discovered adrenal mass. Ann Intern Med 1983;98: 940–945.

78. Dunnick NR. Adrenal carcinoma. Radiol Clin North Am 1994;32:99–108.

79. Francis IR, Korobkin M. Pheochromocytoma. Radiol Clin North Am 1996;34:1101–1112.

80. Bravo EL, Gifford RW. Current concepts: pheochromocytoma—diagnosis, localization and management. N Engl J Med 1984;311: 1298–1303.

81. Sutton MG, Sheps SG, Lie JT. Prevalence of clinically unsuspected pheochromocytoma: review of a 50-year autopsy series. Mayo Clin Proc 1981;56:354–360.

82. Blake MA, Kalra MK, Maher MM, et al. Pheochromocytoma: an imaging chameleon. RadioGraphics 2004;24:S87–S89.

83. Blake MA, Krisnamoorthy SK, Boland GW, et al. Low density pheochromocytoma on CT: a mimicker of adrenal adenoma. AJR Am J Roentgenol 2003;181:1663–1668.

84. Ramsay JA, Asa SL, van Nostrand AW, Hassaram ST, de Harven EP. Lipid degeneration in pheochromocytomas mimicking adrenal cortical tumors. Am J Surg Pathol 1987;11:480–486.

85. Miyajima A, Nakashima J, Baba S, Tachibana M, Nakamura K, Murai M. Clinical experience with incidentally discovered pheochromocytoma. J Urol 1997;157:1566–1568.

86. Raisanen J, Shapiro B, Glazer GM, Desai S, Sisson JC. Plasma catecholamines in pheochromocytoma: effect of urographic contrast media. AJR Am J Roentgenol 1984;143:43–46.

87. Mukherjee JJ, Peppercorn PD, Reznek RH, et al. Pheochromocytoma: effect of nonionic contrast medium in CT on circulating catecholamine levels. Radiology 1997;202: 227–231.

88. Bessell-Browne R, O'Malley ME. CT of pheochromocytoma and paraganglioma: risk of adverse events with IV administration of nonionic contrast material. AJR Am J Roentgenol 2007;188:970–997.

89. Tenenbaum F, Lumbroso J, Schlumberger M, et al. Comparison of radiolabeled octreotide and meta-iodobenzylguanidine (MIBG) scintigraphy in malignant pheochromocytoma. J Nucl Med 1995;36:1–6.

90. Van der Harst E, de Herder WW, Bruining HA, et al. [(123)I] metaiodobenzylguanidine and [(111)In] octreotide uptake in benign and malignant pheochromocytomas. J Clin Endocrinol Metab 2001;86:685–693.

91. Shulkin BL, Thompson NW, Shapiro B, Francis IR, Sisson JC. Pheochromocytomas: imaging with 2-[fluorine-18]fluoro-2-deoxy-D-glucose PET. Radiology 1999;212:35–41.

92. Ilias I, Yu J, Carrasquillo JA, Chen CC, et al. Superiority of 6-[^{18}F]-fluorodopamine positron emission tomography versus [^{131}I] metaiodobenzylguanidine scintigraphy in the localization of metastatic pheochromocytoma. J Clin Endocrinol Metab 2003;88: 4083–4087.

93. Trampal C, Engler H, Juhlin C, Bergström M, Långström B. Pheochromocytomas: detection with ^{11}C hydroxyephedrine PET. Radiology 2004;230:423–428.

94. Burks DW, Mirvis SE, Shanmuganathan K. Acute adrenal injury after blunt abdominal trauma: CT findings. AJR Am J Roentgenol 1992;158:503–507.

95. Xarli VP, Steale AA, Davis PJ, Buescher ES, Rios CN, Garcia-Bunnel R. Adrenal hemorrhage in the adult. Medicine (Baltimore) 1978;57:211–221.

96. Bookstein JJ, Conn J, Reuter SR. Intraadrenal hemorrhage as a complication of adrenal venography in primary aldosteronism. Radiology 1968;90:778–779.

97. Bayliss RI, Edwards OM, Starer F. Complications of adrenal venography. Br J Radiol 1970;43:531–533.

98. Cheema P, Cartegena R, Staubitz W. Adrenal cysts: diagnosis and treatment. J Urol 1981;126:396–399.

99. Tung GA, Pfister RC, Papanicolaou N, Yoder IC. Adrenal cysts: imaging and percutaneous aspiration. Radiology 1989;173:107–111.

100. Feinstein RS, Gatewood OM, Fishman EK, Goldman SM, Siegelman SS. Computed tomography of adult neuroblastoma. J Comput Assist Tomogr 1984;8:720–726.

101. Siegel MJ, Ishwaran H, Fletcher BD, et al. Staging of neuroblastoma at imaging: report of the Radiology Diagnostic Oncology Group. Radiology 2002;223:168–175.

102. Radin R, David CL, Goldfarb H, Francis IR. Adrenal and extra-adrenal retroperitoneal ganglioneuroma: imaging findings in 13 adults. Radiology 1997;202:703–707.

103. Johnson GL, Hruban RH, Marshall FF, Fishman EK. Primary adrenal ganglioneuroma: CT findings in four patients. AJR Am J Roentgenol 1997;169:169–171.

104. Ferrozzi F, Tognini G, Bova D, Zuccoli G, Pavone P. Hemangiosarcoma of the adrenal glands: CT findings in two cases. Abdom Imaging 2001;26:336–339.

105. Kawashima A, Sandler CM, Fishman EK, et al. Spectrum of CT findings in nonmalignant disease of the adrenal gland. RadioGraphics 1998;18:393–412.

106. Krebs TL, Wagner BJ. MR imaging of the adrenal gland: radiologic-pathologic correlation. RadioGraphics 1998;18:1425–1440.

107. Wilson DA, Muchmore HG, Tisdal RG, et al. Histoplasmosis of the adrenal gland studied by CT. Radiology 1984;150:779–783.

108. Morgan HE, Austin JH, Follet DA. Bilateral adrenal enlargement in Addison's disease caused by tuberculosis: nephrotomographic demonstration. Radiology 1975;115:357.

109. Wilms GE, Baert AL, Kint EJ, Pringot JH, Goddeeris PG. Computed tomographic findings in bilateral adrenal tuberculosis. Radiology 1983;146:729.

110. Paulsen SD, Nghiem HV, Korobkin M, Caoili EM, Higgins EJ. Changing role of imaging-guided percutaneous biopsy of adrenal masses: evaluation of 50 adrenal biopsies. AJR Am J Roentgenol 2004;182:1033–1103.

111. Welch TJ, Sheedy PF II, Stephens DH, Johnson CM, Swensen SJ. Percutaneous adrenal biopsy: review of a 10-year experience. Radiology 1994;193:341–344.

112. Silverman SG, Mueller PR, Pinkney LP, Koenker RM, Seltzer SE. Predictive value of image-guided adrenal biopsy: analysis of results of 101 biopsies. Radiology 1993;187:715–718.

113. Mayo-Smith WW, Dupuy DE. Adrenal neoplasms: CT-guided radiofrequency ablation—preliminary results. Radiology 2004;231:225–230.

114. Rhim H, Dodd GD, Chintapalli KN, et al. Radiofrequency thermal ablation of abdominal tumors: lessons learned from complications. RadioGraphics 2004;24:41–52.

115. Lo WK, vanSonnenberg E, Shankar S, et al. Percutaneous CT-guided radiofrequency ablation of symptomatic bilateral adrenal metastases in a single session. J Vasc Interv Radiol 2006;17:175–179.

116. Wood BJ, Abraham J, Hvizda JL, Alexander HR, Fojo T. Radiofrequency ablation of adrenal tumors and adrenocortical carcinoma metastases. Cancer 2003;97:554–560.